J. Phys.: Condens. Matter **12** (2000) 3401–3422. Printed in the UK PII: S0953-8984(00)10452-7

Magnetic and structural instabilities in the stripe-phase region of $La_{1.875}Ba_{0.125-y}Sr_yCuO_4$ ($0 \leqslant y \leqslant 0.1$)

Alexandros Lappas†‡, Kosmas Prassides‡, Fredy N Gygax§ and Alexander Schenck§

† Institute of Electronic Structure and Laser, Foundation for Research and Technology—Hellas, PO Box 1527, Heraklion 711 10, Greece

‡ School of Chemistry, Physics and Environmental Science, University of Sussex, Brighton BN1 9QJ, UK

§ Institute for Particle Physics, Swiss Federal Institute of Technology (ETH) Zurich, CH-5232 Villigen PSI, Switzerland

Received 20 December 1999

Abstract. Zero-field positive muon spin relaxation (ZF-μ^+SR) experiments were performed to investigate the magnetic properties of the low-temperature structural modifications of the $La_{1.875}Ba_{0.125-y}Sr_yCuO_4$ ($y = 0.0$, 0.025, 0.050, 0.075, 0.100) series, in which the total hole concentration is close to 1/8. Together with high-resolution time-of-flight neutron powder diffraction measurements, the results imply that the interplay among lattice distortions, doping and superconductivity is intimately related to the magnetic correlations of the Cu spins, which are interpreted in terms of a stripe-phase model. Materials with $y \leqslant 0.075$ exhibit an incomplete structural transition at T_{d2}, from a low-temperature orthorhombic (LTO, $Bmab$) to a low-temperature tetragonal (LTT, $P4_2/ncm$) phase. Diffraction patterns collected while approaching T_{d2} reveal a rapid reduction of the orthorhombicity in the LTO phase with a residual fraction always surviving to low temperatures. Different behaviour is shown by the composition with $y = 0.1$. Rietveld analysis shows coexistence of the LTO phase with a less distorted low-temperature orthorhombic phase (LTO-2, $Pccn$). In the LTT phase, a fraction of muons senses regions with purely static spin correlations due to an incommensurate spin-density wave. The muon spin depolarization suggests that in the spatially separated remnant LTO, hole-rich domains, dynamical correlations of charge density give rise to superconductivity. As the spin fluctuations become static at $y \leqslant 0.075$, the London penetration depth, λ calculated from the transverse-field μ^+SR depolarization rate, $\sigma(T \to 0) \propto \lambda^{-2} \propto n_s/m^*$, reveals a decrease in the superconducting carrier density. The magnetic freezing temperature, T_f is suppressed and the magnetic phase fraction shrinks as y increases, whereas the superconducting correlations persist in a larger sample volume. The disappearance of long-range magnetic order at $y = 0.1$ and the growth of a quasi-static component correlate well with the presence of the LTO-2 microstructure which behaves as a buffer phase out of which the LTT domains become dominant in the Ba-rich compositions.

1. Introduction

In the quest for high-temperature superconductivity, the relatively simple alkaline-earth- ($M = Ca^{2+}$, Sr^{2+}, Ba^{2+}) doped derivatives of Ln_2CuO_4 (Ln = lanthanide ion) have been studied intensively. They provide good model systems, in which the evolution of the electronic and magnetic properties of the CuO_2 layers as a function of temperature, composition, oxygen ordering and changes in the supporting cation skeleton can be monitored and related to the transition from insulating to metallic to superconducting behaviour. An intriguing situation concerning the inter-relationship of structural anomalies, long-range magnetic ordering and the

0953-8984/00/143401+22$30.00

appearance of superconductivity is shown by the differing phase diagrams of the $La_{2-x}Sr_xCuO_4$ and $La_{2-x}Ba_xCuO_4$ systems in the vicinity of $x \sim 0.125$. Both systems show the presence of a high-temperature tetragonal phase (HTT, space group $I4/mmm$) which undergoes at T_{d1} (∼200 K) a second-order phase transition to a low-temperature orthorhombic phase (LTO, space group $Bmab$) [1]. However, the Ba-doped materials exhibit a further first-order transition to another low-temperature tetragonal structure ($T_{d2} \sim 80$ K) with an enlarged unit cell of dimensions $\sqrt{2}a \times \sqrt{2}a \times c$ (LTT, space group $P4_2/ncm$) [2]. An intriguing feature of the transition, namely a persistent orthorhombic phase at temperatures below T_{d2}, suggestive of domain size effects, was unravelled by neutron structural studies [3].

The interest in these sequences of structural transformations arose from results based on transport and magnetic properties [4], as comparison of Sr^{2+}- and Ba^{2+}-doped La_2CuO_4 materials displayed differences in their superconducting behaviour. The $La_{2-x}Sr_xCuO_4$ series exhibits a smooth evolution of T_c with a maximum near $x = 0.15$ and only a shallow dip around the $La_{1.885}Sr_{0.115}CuO_4$ composition [5]. A distinct behaviour is exhibited by the $La_{2-x}Ba_xCuO_4$ series which shows a pronounced dip in T_c, leading to a non-superconducting composition at $x = 0.125$, followed by a recovery of T_c for $x > 0.125$. The dramatic change in the superconducting properties of these hole-doped materials has been attributed to the subtle structural changes following the LTO → LTT phase transition in the vicinity of $x \sim 0.125$, where T_{d2} reaches a maximum.

Attempts to further our understanding of this behaviour can help to obtain important information on the origin of high-T_c superconductivity. The observation [6] of frozen local Cu^{2+} moments in the LTT phase is consistent with scenarios supporting that antiferromagnetic (AF) correlations in the CuO_2 sheets play an important role in explaining the microscopic mechanism of high-T_c superconductivity. This becomes of great interest when one recalls the competition between magnetism and superconductivity [7] with the long-range AF ordering disappearing upon doping, before the onset of metallic and superconducting behaviour. Later investigations also revealed the presence of the LTO → LTT transformation in closely related materials. The LTT phase is stabilized by Nd substitution with a minimum in T_c encountered for $y \sim 0.12$ in the $La_{2-x-y}Nd_xSr_yCuO_4$ series [8]. Studies of the phase diagram of the $La_{2-x-y}Nd_xSr_yCuO_4$ series for $x > 0.18$ implied a strong influence of the tilt angle of the CuO_6 octahedra in destroying superconductivity and stabilizing local magnetic order in the LTT phase [9, 10]. Electronic [11], spin–orbit coupling [12] and microstructural phase separation [13] models have been proposed to account for the changes in the superconducting properties of materials which undergo the LTO → LTT phase transition.

Considerable interest has been generated by the neutron diffraction work of Tranquada and coworkers [14] on an $La_{1.48}Nd_{0.4}Sr_{0.12}CuO_4$ single crystal. The experimental results revealed that the LTO → LTT transition is accompanied by an incommensurate modulation of spin and charge. More specifically, antiferromagnetic 'stripes' of copper spins were found to be separated periodically by hole-rich regions in which the holes segregate. The implications of these results on the suppression of superconductivity near $x \sim 0.125$ are thus of great interest and have been used to support theoretical expectations [15] that spatial modulations of spin and charge density may be related to superconductivity in the copper oxides.

In an attempt to explore the correlation of the LTT structural anomaly with the detrimental effect on superconductivity, we have undertaken a systematic investigation of the magnetic properties of a series of double-doped samples with stoichiometry $La_{1.875}Ba_{0.125-y}Sr_yCuO_4$ ($y = 0.0$, 0.025, 0.050, 0.075 and 0.100) and varying (Ba/Sr) relative ratios. The studies are combined with the results of high-resolution neutron powder diffraction in order to obtain information on the way the microstructure evolves during the transition from the LTO to the LTT phase. It had been reported before that even though the hole-doping level is kept

close to (1/8), T_c increases in this series essentially monotonically with increasing y, i.e. decreasing (Ba/Sr) ratio [16, 17]. In this work, we report on the interplay between structural and magnetic instabilities and superconductivity through the results of zero-field muon spin relaxation measurements (ZF-μ^+SR) in the temperature range 0.06 K $\leqslant T \leqslant$ 100 K, which extends across the LTO to the LTT phase boundaries, determined by neutron powder diffraction.

2. Experimental details

Polycrystalline samples with composition $La_{1.875}Ba_{0.125-y}Sr_yCuO_4$ ($y = 0.0$, 0.025, 0.050, 0.075 and 0.100) were prepared by the usual solid state method of mixing stoichiometric amounts of oxides and carbonates of the constituent metallic elements and then repeatedly regrinding and annealing the pelletized powders at high temperature. The samples were characterized by x-ray powder diffraction with a Siemens D-5000 diffractometer and the oxygen content was determined to be close to the stoichiometric value ($\delta \sim 0$) by combining the results of thermogravimetric analysis and iodometric titrations. The transition to the superconducting state was determined by means of both four-probe ac resistivity and SQUID susceptibility measurements. The critical temperature, T_c for the onset of superconductivity increases linearly with increasing Sr^{2+} content [17], from ∼13 K for $y = 0.0$ to ∼28 K for $y = 0.1$.

Temperature dependent structural work was undertaken with the high-resolution neutron powder diffractometer, HRPD at ISIS, Rutherford Appleton Laboratory, UK. 10 g of the material were placed in a rectangular vanadium sample holder and positioned in a liquid helium cryostat, accessing the temperature range 4.5 to 300 K. The lower resolution, 1 m sample position, was used in these measurements, with backscattering and 90° detector banks being monitored simultaneously. With HRPD operating at 25 μA h^{-1} current, improved statistics were achieved for the 4.5 K data sets of $La_{1.875}Ba_{0.125-y}Sr_yCuO_4$ compositions with $y = 0.025$ (duration of run ∼4.2 h), $y = 0.050$ (∼3.9 h) and $y = 0.100$ (∼1.8 h). The phasing of HRPD choppers was such that the time-of-flight window between 30 and 130 ms, equivalent to d-spacing range (0.62–2.69) Å, could be observed, with good signal to noise ratio and superb resolution at short d-spacings. Additional diffraction profiles were collected at elevated temperatures for $La_{1.875}Ba_{0.100}Sr_{0.025}CuO_4$ at 120 K with 38.4 μA total current and for $La_{1.875}Ba_{0.075}Sr_{0.050}CuO_4$ at 120 and 300 K with 48.7 and 22.1 μA total current, respectively.

In order to study the structural transformations in more detail, rapid scans over a time-of-flight window of (40–140) ms, corresponding to a d-spacing range of (0.83–2.90) Å were also performed. 30 min runs were recorded between 10 and 70 K in 3 K steps for $La_{1.875}Ba_{0.100}Sr_{0.025}CuO_4$, while 20 min runs were obtained in steps of 2 K between 8 and 16 K and thereafter in steps of 3 K up to 52 K for $La_{1.875}Ba_{0.075}Sr_{0.050}CuO_4$. For every step, the temperature was left to stabilize for 10 minutes before initializing the counting electronics. The data were normalized to the incident beam, corrected with a standard vanadium run to account for detector efficiency and analysed using the GSAS [18] suite of programs. Prior to the Rietveld refinements, the high statistics runs were rebinned in steps of 0.0003 μs within the measured time-of-flight window, while the ones collected during temperature ramping were rebinned in steps of 0.0002 μs.

This study offered a unique opportunity to relate the changes in the conducting properties to the structural transformations [19]. All samples with $y \leqslant 0.075$ undergo a transition to the LTT phase at different onset temperatures, T_{d2}, depending on the Ba content. Muon spin rotation measurements in transverse field (TF-μ^+SR) were able to probe the superconducting state below the transition to the LTT phase; our early studies on a $y = 0.050$ sample

($T_{d2} \approx 46$ K) found that the depolarization of the muon spin was achieved via two independent channels. Only a small volume fraction of the sample was superconducting, while the dominant contribution came from the part of the sample, which was in a magnetically ordered state [20].

The problem of the existence of static magnetic local fields in the low-temperature phases of $La_{1.875}Ba_{0.125-y}Sr_yCuO_4$ is addressed in this work by using 100% spin-polarized positive muons (μ^+) in the absence of external fields. The μ^+SR experiments were carried out at the Paul Scherrer Institute, Villigen, Switzerland, using both a ^{3}He–^{4}He dilution refrigerator (LTF spectrometer) and an He-flow cryostat (GPS spectrometer) on the μ^+SR dedicated πM3 beamline of the PSI-600 MeV proton accelerator. The powdered samples were pressed into pellets and attached to the cryostat cold finger. Typical scans of ~30 min covered the temperature range of interest. The muons are implanted in the solid sample and after they come to rest at an interstitial site, they act as highly sensitive microscopic local magnetic probes. In the presence of local magnetic fields, $\langle B_\mu \rangle$, they will precess with a frequency, $\nu_\mu = (\gamma_\mu/2\pi)\langle B_\mu \rangle$, where $(\gamma_\mu/2\pi) = 13.55$ kHz G^{-1} is the muon gyromagnetic ratio. In the absence of an applied external field (ZF-μ^+SR), the appearance of precession implies the onset of a magnetic ordering transition. Moreover, application of a magnetic field parallel to the initial muon spin polarization (longitudinal field) allows the decoupling of the μ^+-spin from the static internal field components. In transverse-field (TF-) μ^+SR, an external magnetic field, H_{ext} applied perpendicular to the previous direction results in a precession signal for the μ^+-spin. In the mixed state of superconducting materials, the external field ($B_{c1} \ll B_{ext} \ll B_{c2}$) penetrates the sample in the form of flux vortices and gives rise to a local magnetic field, B which has a distribution with a width ΔB proportional to λ^{-2} [21, 22]. This method has been extensively used in the study of the London penetration depth, λ in various type-II superconductors [23, 24]. We employed TF-μ^+SR in field-cooling ($B_{ext} = 6$ kG) experiments for the two end-compositions ($y = 0.0$, 0.1) to measure the depolarization rate, σ ($\propto \Delta B \propto \lambda^{-2}$) due to the inhomogeneous field distribution of the vortex state below T_c. The μ^+SR technique in its various variants has proven extremely powerful in the field of small-moment magnetism and, in all cases, when magnetic order is of random, very short-range, spatially inhomogeneous or incommensurate nature [25].

3. Results and discussion

3.1. Neutron full profile analysis—determination of the structure type

The $La_{1.875}Ba_{0.125-y}Sr_yCuO_4$ systems adopt structures related to the K_2NiF_4 structural type. The polymorphism in such layered perovskite structures has been demonstrated in many experimental [2, 26] and theoretical studies [27]. Accordingly the diffraction profiles collected for the $y = 0.025$, 0.050 and 0.100 compositions at low (4.5 K), intermediate (120 K) and high (300 K) temperatures should be described using the $I4/mmm$ space group or one of its Landau subgroups, $Bmab$, $Pccn$ and $P4_2/ncm$. This variation in the crystallographic symmetry reflects the possible modes of rotation of the octahedral CuO_6 units. Axe *et al* [2, 28] have shown that the sequence of structural transformations can be understood by expanding the Landau–Ginzburg free energy (corresponding to a simple thermodynamic potential) in terms of a degenerate pair of primary order parameters, Q_1, Q_2, which describe the soft phonon tilts around the [110] and [1$\bar{1}$0] axes of the undistorted $I4/mmm$ structure, respectively. With Q_1 and Q_2 related to the amplitude of the tilting distortion, the following structural phases are possible: HTT ($Q_1 = Q_2 = 0$), LTO ($Q_1 \neq 0$, $Q_2 = 0$ or $Q_1 = 0$, $Q_2 \neq 0$), LTT ($|Q_1| = |Q_2| \neq 0$) and LTO-2 ($Q_1 \neq 0$, $Q_2 \neq 0$, $Q_1 \neq Q_2$).

For all samples in the present study, Rietveld refinements were carried out with the GSAS code using a peak-shape function involving the convolution of a pseudo-Voigt with back-to-back exponentials. A random distribution of the Ba/Sr cations at the rare-earth site was assumed, according to the nominal composition of the material; initial refinements included the scale factor and the coefficients of a fifth-order Chebyshev polynomial accounting for the background scattering. Then, the lattice parameters, the fractional coordinates of the atoms, the absorption correction parameters and the isotropic temperature factors were left free to change successively. When stable refinements were achieved, the Gaussian and Lorentzian broadening parameters relating to the peak shape function were also refined. At this stage, the occupancies of the oxygen atoms were not found to deviate significantly from their nominal values. Therefore, they were kept constant at their stoichiometric values. After this procedure was complete, inspection of the profiles revealed that the peaks which were not clearly accounted for were those due to the sample environment (e.g. cryostat and vanadium sample holder: $d \sim 2.13$, 1.23 Å).

The overall structural picture is consistent with the sequence of phase transitions described above. Qualitatively, on lowering the temperature there is a bond-length mismatch between adjacent rock-salt $(La,Ba,Sr)_2O_2$ bilayers and the CuO_2 planes. The resulting compressive stress on the Cu–O layers is relieved by a gradual rotation of the CuO_6 octahedra around either the $[110]_{HTT}$ or $[1\bar{1}0]_{HTT}$ tetragonal axes. The effect of this tilting distortion is the transformation (at T_{d1}) of the HTT phase to the LTO structure. Indexing of superlattice reflections which appeared in the diffraction patterns of $y = 0.025$, 0.050 at 120 K (and $y = 0.100$ at 4.5 K) was carried out on the basis of a $\sqrt{2}a \times \sqrt{2}b \times c$ supercell of the HTT phase. In this case, neighbouring octahedra in the (100) planes are contra-rotated, whereas those in (110) planes are co-rotated. Furthermore, our neutron diffraction data (e.g. $y = 0.025$, 0.050 at 4.5 K) support a further low-temperature transformation which is accompanied by a sharp change in the orthorhombic strain. Systematic absences of reflections such as $(h0l)$ with $h + l = 2n + 1$ allow description of the structure o0n an enlarged and rotated unit cell of dimensions $\sqrt{2}a \times \sqrt{2}a \times c$ with respect to the HTT phase (LTT phase, $P4_2/ncm$). A marked broadening of the Bragg peaks accompanies this transformation with the transition temperature (T_{d2}) strongly dependent on the Sr^{2+} doping level.

The sequence of phase transitions, HTT $\rightarrow$ LTO $\rightarrow$ LTT is demonstrated clearly by $La_{1.875}Ba_{0.075}Sr_{0.050}CuO_4$; the room-temperature diffraction profile refines well with the HTT structure (figure 1(a)). The diffraction profile at 120 K shows that the material adopts orthorhombic $Bmab$ symmetry (LTO) (figure 1(b)). The orthorhombic distortion is $(b-a)/(b+a) = 2.083(8) \times 10^{-3}$. At 4.5 K, despite the systematic hkl-dependent broadening of the Bragg peaks, the $P4_2/ncm$ symmetry accounts for all the observed reflections; however, the quality of the fit was only moderately good, resulting in $R_{wp} = 10.9\%$ ($\chi^2 = 31.4$). In particular, $h0l$ reflections were observed to be broader than calculated, whereas hhl reflections narrower. Figure 2(a) presents a short time-of-flight window (corresponding to $d \approx 1.274$–1.482 Å) of the difference profile resulting after single-phase Rietveld refinements. The normalized difference is large due to marked anisotropic broadening of different families of hkl-reflections. A statistically significant improvement of the quality of the fit is achieved ($R_{wp} = 5.4\%$; $\chi^2 = 7.8$) when a two-phase crystallographic model is used with 46.3(8)% of the total sample volume remaining in the LTO phase. The refined parameters and the agreement factors between observed and calculated profiles are compiled in table 1. Selected bond distances and copper–oxygen bond angles are presented in table 2.

Rietveld refinements of the neutron powder diffraction patterns of $La_{1.875}Ba_{0.100}Sr_{0.025}CuO_4$ followed the same route. A splitting of the diffraction peaks characteristic of the LTO phase was present at 120 K ($a = 5.343\,47(4)$ Å, $b = 5.362\,79(4)$ Å, $c = 13.242\,49(9)$ Å) with

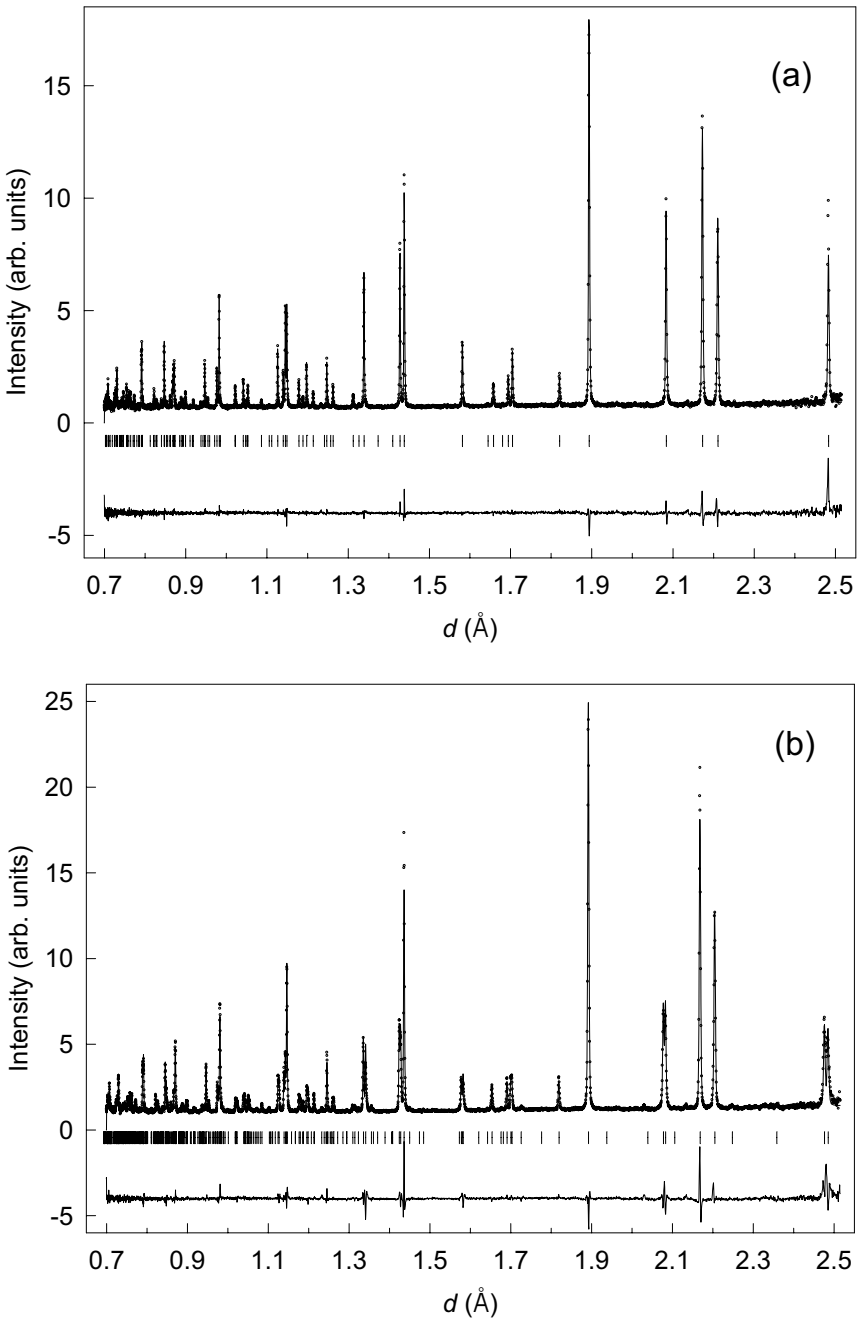

Figure 1. Observed (points), calculated (full curve) and difference neutron time-of-flight diffraction profiles of $La_{1.875}Ba_{0.075}Sr_{0.050}CuO_4$, after Rietveld refinements of: (a) the HTT phase (T = 300 K, space group $I4/mmm$); (b) the LTO phase (T = 120 K, space group $Bmab$); (c) the coexisting LTT and LTO phases (T = 4.5 K, space groups $P4_2/ncm$, $Bmab$ and reflection positions marked by the top and bottom set of ticks, respectively).

a smaller orthorhombic distortion $(b-a)/(b+a) = 1.805(8) \times 10^{-3}$. Similar behaviour to that of the $y = 0.050$ compound is observed below the transition, T_{d2} to the LTT phase (figure 2(b)).

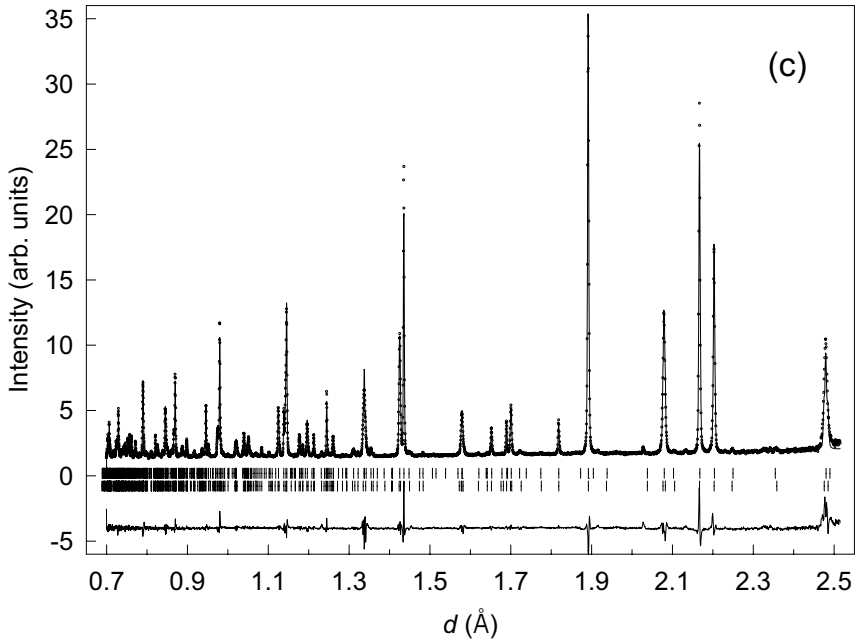

Figure 1. (Continued)

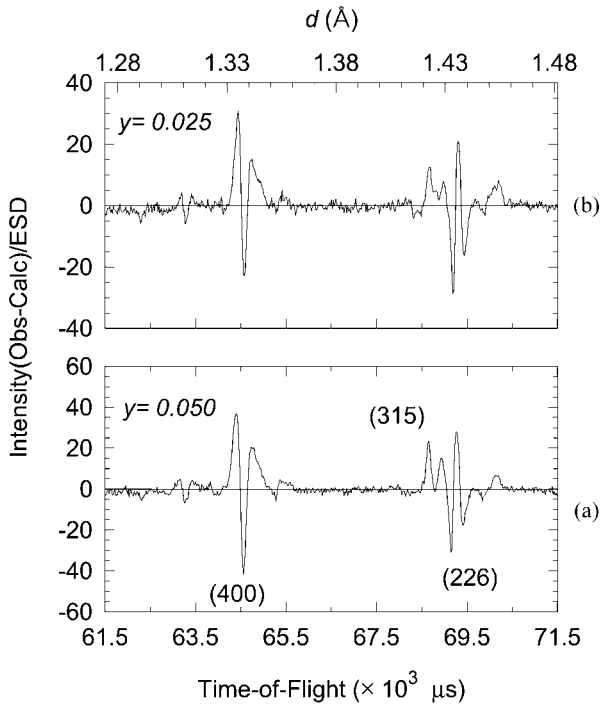

Figure 2. Difference profile of $La_{1.875}Ba_{0.125-y}Sr_yCuO_4$ at 4.5 K ($y = 0.025$ and $y = 0.050$) after single-phase Rietveld refinements of the LTT phase (space group $P4_2/ncm$), showing the large estimated standard deviations (ESDs) due to anisotropic hkl-broadening.

While the LTT phase is dominant again at 4.5 K ($a = b = 5.352\,37(3)$ Å, $c = 13.2308(2)$ Å), a fraction of 37.6(8)% of the LTO phase ($a = 5.3439(1)$ Å, $b = 5.3594(1)$ Å, $c = 13.2402(3)$ Å) is again needed to describe best the diffraction profile.

3.2. Optimization of the structural model—composition dependence

Analysis of the diffraction data of $La_{1.875}Ba_{0.025}Sr_{0.100}CuO_4$ at 4.5 K revealed a large orthorhombic distortion, $(b - a)/(b + a) = 2.980(16) \times 10^{-3}$ with the $Bmab$ space group leading to agreement factors, $R_{wp} = 10.4\%$, $\chi^2 = 13.5$. However, large ESD in the Rietveld difference plots implied that a single-phase LTO model was still inadequate. A systematic search for the presence of a second phase led to the LTO-2 phase (space group $Pccn$) as the best candidate to account for the missing intensity of many Bragg reflections. The two-phase Rietveld refinement led to a significant improvement in the quality of the fit, with $R_{wp} = 7.6\%$, $\chi^2 = 7.1$; the fraction of the LTO-2 phase refined to 48.5(8)%. This strongly supports the view that the sample is composed of a mixture of orthorhombic phases in the microscopic level. However, following this, additional inspection of the fitted diffraction profile revealed that a number of Bragg reflections could not be still described adequately despite careful refinements of the broadening parameters (of Gaussian, σ and Lorentzian, γ shapes) of the pseudo-Voigt profile function, for each of the orthorhombic phases. For example, as shown in the inset of figure 3, the set of hhl reflections is poorly fitted. A significantly better fit ($R_{wp} = 6.3\%$, $\chi^2 = 5$) to the data was achieved when superlattice peaks attributed to the LTT phase were also taken into account. Figure 3 presents the result of the final three-phase Rietveld refinement, which incorporates a small minority LTT volume fraction (∼11.6(3)%) together with those of the majority orthorhombic LTO-2 (∼56.8(7)%; $(b-a)/(b+a) = 2.563(19) \times 10^{-3}$) and LTO (∼31.6(3)%; $(b - a)/(b + a) = 4.389(37) \times 10^{-3}$) phases in $La_{1.875}Ba_{0.025}Sr_{0.100}CuO_4$. The resulting structural parameters are given in table 1 with selected bond distances and angles in table 2.

The appearance of the LTO-2 microstructure in the Sr-rich end of the solid solutions highlights the important role that the relative Ba/Sr content plays in determining the progressive growth of the LTT structure. This is reminiscent of the analogous composition dependence of the $La_{2-x-y}Nd_xSr_yCuO_4$ series at low Sr doping [29]. It seems that the $Pccn$ structure acts as a buffer phase out of which LTT microdomains eventually become the dominant volume fraction of the materials. The evolution of the microstructure in $La_{1.875}Ba_{0.125-y}Sr_yCuO_4$, with the involvement of the $Pccn$ structure is not surprising in view of earlier electron microscopy results, which had suggested [30] a similar behaviour for $La_{1.88}Ba_{0.12}CuO_4$ with the transition occurring from LTO → LTT via LTO-2. It is of interest to note the Ba/Sr concentration dependence of the tilts of copper–oxygen octahedra in LTT and LTO-2 phases, respectively. The average buckling angle (of the O–Cu–O bonds) of the copper–oxygen planar bonds changes from $\theta = 3.28^\circ$ for $y = 0.025$, to $\theta = 2.48^\circ$ for $y = 0.05$, and to $\theta = 1.06^\circ$ for $y = 0.1$ (in this case there are two non-equivalent in-plane oxygen atoms resulting in $\theta_{O_{(2)}} = 0.56^\circ$ for one and $\theta_{O_{(3)}} = 1.56^\circ$ for the other). Buchner *et al* [9] argued that in Nd-doped $La_{2-x}Sr_xCuO_4$, superconductivity disappears in the LTT phase only for $\phi_{critical} > 3.6^\circ$. This is at odds with the behaviour in $La_{1.875}Ba_{0.125-y}Sr_yCuO_4$ since, as we discuss below, superconductivity is not supported in the LTT phase even for values of $\phi < 3.6^\circ$.

An important feature of this analysis is that the low-temperature structure of $La_{1.875}Ba_{0.125-y}Sr_yCuO_4$ is not consistent with a single phase LTT model (figure 2). This is not true for the HTT phase where the $I4/mmm$ space group leads to excellent quality of fit (figure 1(a)). Similar observations by means of high-resolution synchrotron x-ray and neutron powder diffraction have been reported in the literature for the low-temperature structural

Table 1. Final structural parameters derived from multi-phase ($T = 4.5$ K) and single-phase ($T = 120$, 300 K) Rietveld refinements of $La_{1.875}Ba_{0.125-y}Sr_yCuO_4$. N, P represent the total number of observations and basic variables, respectively. R is the number of Bragg reflections. Numbers in parentheses indicate the estimated standard deviation in the last digit.

		y, T (K), counting time (h)						
		0.050, 4.5, 3.9		0.050, 120, 1.9	0.050, 300, 0.9	0.100, 4.5, 1.8		
		$P4_2/ncm$	$Bmab$	$Bmab$	$I4/mmm$	$P4_2/ncm$	$Pccn$	$Bmab$
Weighted fraction		53.6(8)%	46.4(8)%	100%	100%	11.6(3)%	56.8(7)%	31.6(3)%
a (Å)		5.350 50(4)	5.339 59(8)	5.341 07(4)	3.787 45(1)	5.3335(2)	5.3327(1)	5.3309(2)
b (Å)		5.350 50(4)	5.363 74(9)	5.363 37(4)	3.787 45(1)	5.3335(2)	5.3601(1)	5.3779(2)
c (Å)		13.2227(2)	13.2180(3)	13.229 06(8)	13.264 74(5)	13.2296(7)	13.2032(2)	13.1869(3)
V (Å^3)		378.538(8)	378.566(11)	378.961(5)	190.279(1)	376.328(25)	377.399(7)	378.061(12)
La/Ba/Sr	x	0.0047(5)	0.5	0.5	0.0	0.006	0.0004(20)	0.5
	y	0.0047(5)	0.0061(9)	0.00489(9)	0.0	0.006	0.0044(8)	0.0086(11)
	z	0.360 87(25)	0.360 40(29)	0.360 70(9)	0.360 60(7)	0.3613(9)	0.360 85(32)	0.360 37(43)
	U_{iso} (Å^2)	0.0024(9)	0.0018(10)	0.0024(5)	0.0063(4)	0.0032(18)	0.0035(7)	0.0004(7)
Cu	U_{iso} (Å^2)	0.0038(10)	−0.0013(11)	0.0013(5)	0.0049(4)	0.0032(18)	0.0035(7)	0.0004(7)
O(1)	x	−0.0212(6)	0.5	0.5	0.0	−0.0258(30)	0.0103(29)	0.5
	y	−0.0212(6)	−0.0269(9)	−0.0260(5)	0.0	−0.0258(30)	0.4721(8)	−0.0310(11)
	z	0.1823(4)	0.1829(5)	0.182 55(14)	0.182 64(11)	0.1789(15)	0.3171(5)	0.1833(7)
	U_{iso} (Å^2)	0.0073(11)	0.0064(12)	0.0079(6)	$U_{11} = U_{22} = 0.0235(5)$ $U_{33} = 0.0067(7)$	0.0032(18)	0.0035(7)	0.0004(7)
O(2)	z	0.0062(11)	0.0047(9)	0.0041(4)	0.0	0.0082(34)	−0.0014(14)	0.0073(8)
	U_{iso} (Å^2)	0.0008(29)	0.0035(12)	0.0056(6)	$U_{11} = 0.0100(7)$ $U_{22} = 0.0055(7)$ $U_{33} = 0.0151(9)$	0.0032(18)	0.0035(7)	0.0004(7)
O(3)	z	0.0	—	—	—	0.0	−0.0039(18)	—
	U_{iso} (Å^2)	0.0152(39)	—	—	—	0.0032(18)	0.0035(7)	—
R_{wp}, R_p		5.38%, 4.50%		6.22%, 5.05%	5.09%, 4.99%		6.30%, 5.16%	
χ^2		7.74		5.32	1.59		4.98	
N, P, R		4268, 35, 681		4268, 21, 333	4268, 21, 118		4282, 37, 1296	

The atoms were refined in the following positions in the unit cell:
Space group $P4_2/ncm$: 8(La/Ba/Sr) and 8O(1) in (i) (..m): x, x, z. 4Cu in (d) (..2/m): 0, 0, 0. 4O(2) in (e) (2.mm): 1/4, 1/4, z. 4O(3) in (a) (2.22): 3/4, 1/4, 0.
Space group $Bmab$: 8(La/Ba/Sr) and 8O(1) in (f) (m..): 1/2, y, z. 4Cu in (a) (2/m..): 1/2, 0, 0. 8O(2) in (e) (.2.): 1/4, 1/4, z.
Space group $I4/mmm$: 4(La/Ba/Sr) and 4O(1) in (e) (4mm): 0, 0, z. 2Cu in (a) (4/mmm): 0, 0, 0. 4O(2) in (c) (mmm.): 0, 1/2, 0.
Space group $Pccn$: 8(La/Ba/Sr) and 8O(1) in (e) (1): x, y, z. 4Cu in (a) ($\bar{1}$): 0, 0, 0. 4O(2) in (c) (..2): 1/4, 1/4, z. 4O(3) in (d) (..2): 1/4, 3/4, z.

Table 2. Selected bond distances (Å) and angles (°) for $La_{1.875}Ba_{0.125-y}Sr_yCuO_4$ from multiphase ($T = 4.5$ K) and single-phase ($T = 120$, 300 K) Rietveld refinements of neutron powder diffraction data.

	y, T (K)						
	0.050, 4.5		0.050, 120	0.050, 300	0.100, 4.5		
	$P4_2/ncm$	$Bmab$	$Bmab$	$I4/mmm$	$P4_2/ncm$	$Pccn$	$Bmab$
Cu–O(1) (ax)	2.416(5) × 2	2.421(6) × 2	2.419(2) × 2	2.423(1) × 2	2.375(20) × 2	2.421(7) × 2	2.423(9) × 2
Cu–O(2) (eq)	1.8934(7) × 2	1.8931(4) × 4	1.893 06(13) × 4	1.893 72(0) × 4	1.8888(26) × 2	1.890 34(18) × 2	1.8955(5) × 4
Cu–O(3) (eq)	1.891 69(1) × 2	—	—	—	1.885 67(6) × 2	1.8909(6) × 2	—
O(2)–Cu–O(2)	179.972(0)	180.0	180.0	179.980(0)	180.000(0)	180.0	180.0
O(2)–Cu–O(1)	91.3(5)	90.5(4)	90.7(2)	90.0	91.4(15)	94.0(6)	90.11(35)
O(3)–Cu–O(1)	90.0	90.5(4)	90.7(2)	90.0	90.0	90.1(7)	90.11(35)
O(2)–Cu–O(3)*	90.0	90.32(2)	90.285(8)	90.0	90.0	90.279(18)	90.650(33)
Cu–O(2)–Cu	175.1(9)	176.2(7)	176.8(3)	179.980(0)	173.4(27)	178.9(11)	174.2(6)
Cu–O(3)–Cu	179.980(0)	—	—	—	180.0	176.9(14)	—
(La/Ba/Sr)–O(1)	2.369(7) × 1	2.354(8) × 1	2.363(3) × 1	2.361(2) × 1	2.425(26) × 1	2.356(8) × 1	2.345(12) × 1
	2.602(4) × 2	2.569(6) × 1	2.580(3) × 1	2.7389(3) × 4	2.556(15) × 2	2.573(6) × 1	2.542(7) × 1
	2.872(4) × 2	2.7325(15) × 2	2.7335(4) × 2		2.887(17) × 2	2.676(20) × 1	2.7296(21) × 2
		2.915(6) × 1	2.904(3) × 1			2.787(21) × 1	2.958(7) × 1
						2.912(6) × 1	
(La/Ba/Sr)–O(2)	2.608(11) × 1	2.616(9) × 2	2.618(3) × 2	2.6468(6) × 4	2.589(31) × 1	2.610(14) × 1	2.599(9) × 2
	2.672(11) × 1	2.671(9) × 2	2.666(3) × 2		2.677(34) × 1	2.662(14) × 1	2.686(9) × 2
(La/Ba/Sr)–O(3)	2.639(2) × 2	—	—	—	2.631(8) × 2	—	
						2.661(18) × 1	
Average (La/Ba/Sr)–O	2.653(5)	2.653(7)	2.654(2)	2.6560(6)	2.649(19)	2.650(14)	2.653(7)

* In the parent tetragonal ($I4/mmm$) and orthorhombic ($Bmab$) phases the basal plane oxygen atoms are crystallographically equivalent, and therefore the corresponding bond lengths and angles given correspond to the O(2) type of atoms. ax = axial and eq = equatorial oxygen atoms.

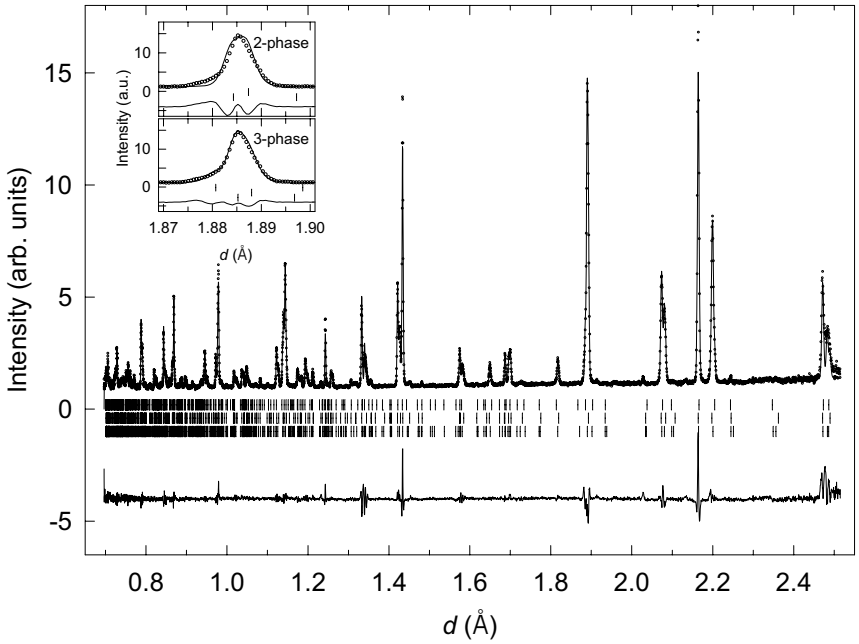

Figure 3. Observed (points), calculated (full curve), and difference neutron time-of-flight diffraction profiles of $La_{1.875}Ba_{0.025}Sr_{0.100}CuO_4$ at $T = 4.5$ K, after three-phase Rietveld refinements. The tick marks show the reflection positions for the LTT (top set), LTO (middle set) and LTO-2 (bottom set) phases, described by space groups: $P4_2/ncm$, $Bmab$ and $Pccn$, respectively. Inset: indicative narrow d-spacing region displaying the improvement of the Rietveld fit to the data after incorporating a third minority LTT phase (bottom panel) to account for the missing intensity of the hhl peaks in two-phase refinements (top panel).

transformations of $La_{2-x}Ba_xCuO_4$ [2, 31], La_2NiO_4 [32] and the rare-earth-substituted $(La,RE)_{2-y}Sr_yCuO_4$ (RE = Nd, Sm) [8, 33]. Residual micro-strain effects accompanying the LTO $\rightarrow$ LTT structural transformation were considered responsible for the presence of strong anisotropic broadening of the Bragg peaks.

Full profile Rietveld refinements were performed with the previous two-phase model for all diffraction patterns collected between 10 and 70 K and 8 and 52 K for $y = 0.025$ and 0.050, respectively. The atomic positions were constrained to the values found at 4.5 and 120 K, while the scale factor, background coefficients, relative fractions of the two phases, lattice constants and peak shape parameters were refined. The orthorhombic distortion of the LTO phase reduces sharply at T_{d2} (figure 4). On cooling to $T_{d2} \approx 61$ K for $y = 0.025$ and $T_{d2} \approx 46$ K for $y = 0.050$, the intensity of the orthorhombic (hkl) doublets decreases gradually and new peaks due to the tetragonal phase appear. The latter grow in intensity as the temperature is lowered. Even with the high resolution of HRPD, the tetragonal reflections (e.g. (400) and (315) in figure 2) appear to be considerably broad even at the lowest temperature measured; this was suggestive of some co-existing, residual proportion of the LTO phase. Thus on approaching T_{d2}, a sudden but steady increase of the LTT volume fraction at $T \leqslant 61$ K and $T \leqslant 46$ K for $y = 0.025$ and 0.050, respectively occurs (figure 4). This always grows at the expense of the LTO phase and results in a dominant LTT phase at low temperatures. Thus the two phases co-exist over a wide temperature range with their respective volume fractions found to saturate below about 40 K for $y = 0.025$ and 19 K for $y = 0.050$.

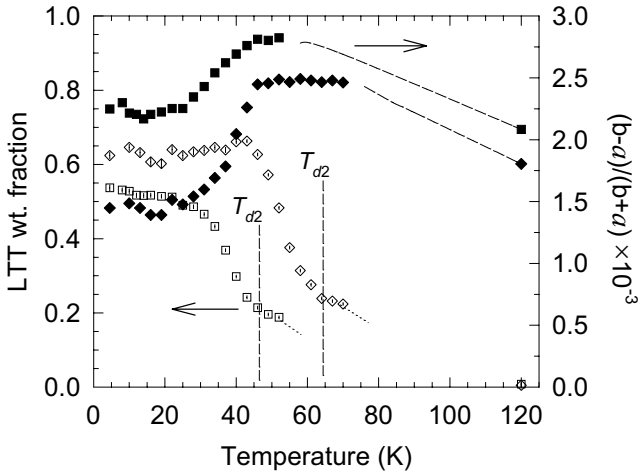

Figure 4. Temperature evolution of (i) the weighted volume fraction of the LTT phase in $La_{1.875}Ba_{0.125-y}Sr_yCuO_4$ ($y = 0.025$ (◇), 0.050 (□)), (left-hand side axis) and (ii) the orthorhombic distortion of the LTO phase close to and below the LTO → LTT structural transformation (at T_{d2}) ($y = 0.025$ (◆), 0.050 (■)) (right-hand side axis). Both quantities were calculated from the Rietveld analysis of the neutron data.

3.3. Static magnetic local fields—muon spin relaxation

For $y \leqslant 0.075$, the ZF-μ^+SR data clearly reveal long-lived oscillations due to coherent Larmor precession of the muon spin. This implies that the systems undergo a transition to a magnetically ordered state in which the localized Cu^{2+} electronic moments are static. ZF-μ^+SR measurements show that the static order is of long-range nature with a characteristic freezing temperature, T_f, which is a sensitive function of the relative (Ba/Sr) content. Figure 5 shows representative time-dependent muon spectra for two members of the $La_{1.875}Ba_{0.125-y}Sr_yCuO_4$ family with $y = 0.025$ (figure 5(a)) and $y = 0.075$ (figure 5(b)) at 300 mK, together with spectra at selected temperatures while approaching T_f.

Below T_f, the appearance of the oscillatory signal is accompanied by a significant increase of an order of magnitude ($\sigma \sim 10\ \mu s^{-1}$) of the respective relaxation rate. In order to describe the shape of the time-dependent ZF-μ^+SR spectra in this temperature range, the following function was employed:

$$P_\mu(t) = [A_\perp \exp(-\tfrac{1}{2}\sigma_1^2 t^2) J_0(2\pi \nu_\mu t) + A_\parallel \exp(-\lambda_2 t)] + A_{nm} \exp(-\lambda_3 t) \quad (1)$$

shown as a solid line through the data in figure 5. $A_\perp$, $A_\parallel$ and A_{nm} are amplitudes reflecting the magnetic and non-magnetic fractions of the muons contributing to the depolarization of the muon spin, ν_μ is the Larmor frequency of the coherent μ^+ precession and σ_1, λ_2 and λ_3 are relaxation rates associated with the three components. The spontaneous, oscillating signal is described by component No 1. The use of the damped J_0 Bessel function to describe the oscillations was preferred over the simple oscillating term, $P_\mu(t) \sim \exp(-\frac{1}{2}\sigma_1^2 t^2) \cos(2\pi \nu_\mu t + \phi)$ [34] because the latter led to unphysically large values [35] of 18–45° for the phase ϕ. The second term in equation (1) arises from the fact that for a completely random distribution of directions of the internal field in a homogeneous polycrystalline sample, one-third of all muons will experience an internal field along their initial spin direction and therefore will not precess. This gives rise to a slowly relaxing contribution (for example at $T = 300$ mK: $\lambda_2 = 0.16(3)\ \mu s^{-1}$ for $y = 0.025$ and

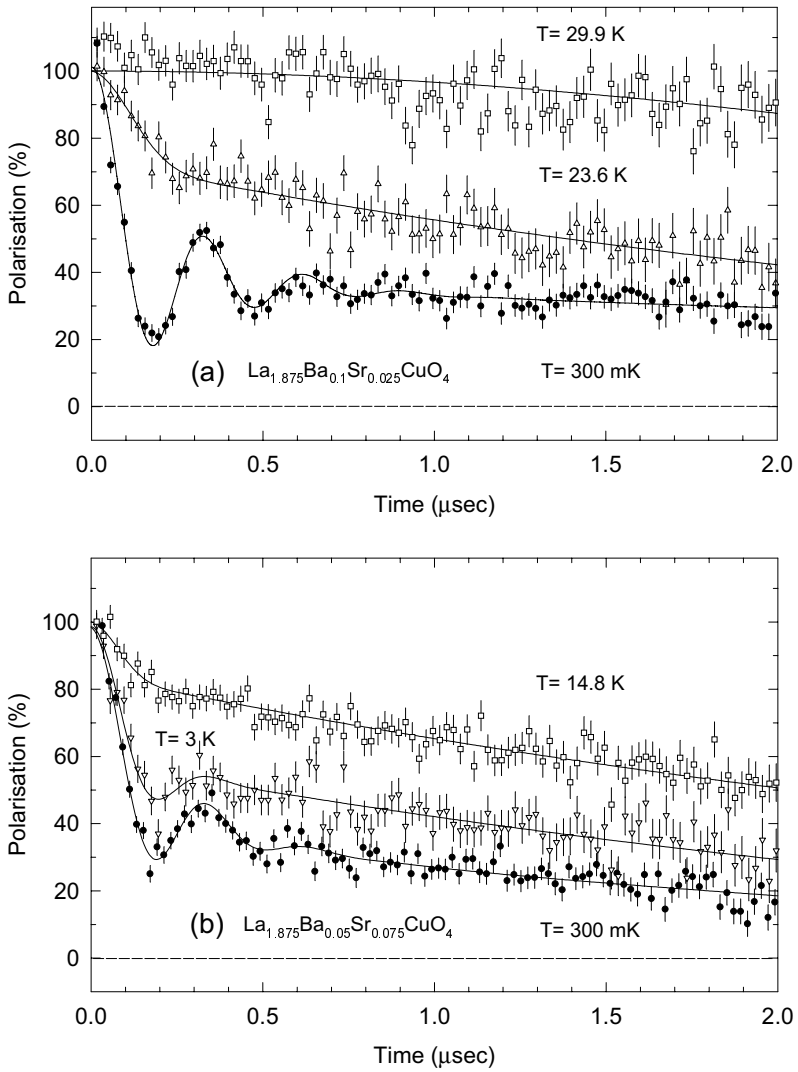

Figure 5. Time evolution of the ZF μ^+-spin polarization, $P_\mu(t)$ in polycrystalline (a) $La_{1.875}Ba_{0.100}Sr_{0.025}CuO_4$ and (b) $La_{1.875}Ba_{0.050}Sr_{0.075}CuO_4$ at various temperatures. The solid lines represent fits to the data with a multicomponent function, which employs a J_0 Bessel function below the transition to the magnetically ordered state. Just above the transition the data are modelled by the sum of a Gaussian and Lorentzian field distribution. At high temperatures, a single Gaussian component is used.

$\lambda_2 = 0.47(5)\ \mu s^{-1}$ for $y = 0.075$), with λ_2 being an estimate of the longitudinal field inhomogeneities. For the purposes of the non-linear least-squares analysis of the present ZF-μ^+SR data, we fixed the ratio of the amplitudes to the ideal value, $A_\parallel/A_\perp = 1/2$. The third term in equation (1) (A_{nm}, component No 2) is of non-magnetic origin. It represents the paramagnetic regions of the sample which produce relatively faster depolarization of the muon spin (for example at $T = 300$ mK: $\lambda_3 = 1.2(4)\ \mu s^{-1}$ for $y = 0.025$ and $\lambda_3 = 2.6(4)\ \mu s^{-1}$ for $y = 0.075$).

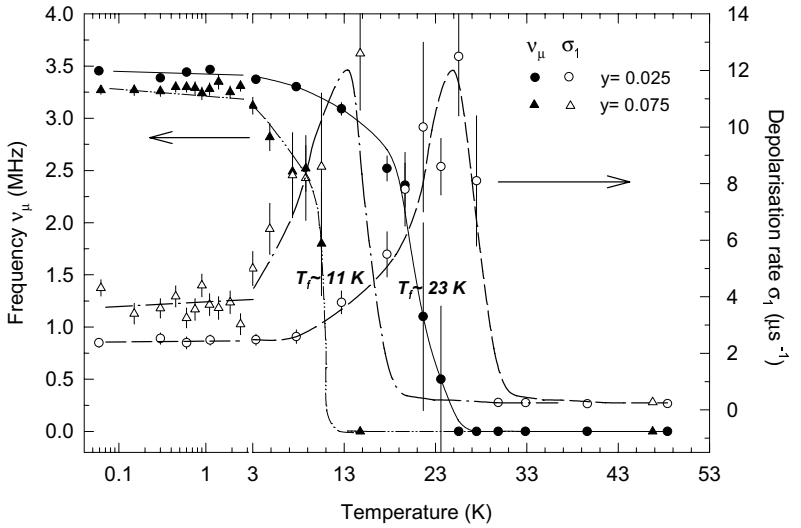

Figure 6. Temperature evolution of the ZF-μ^+SR spontaneous frequency, ν_μ in $La_{1.875}Ba_{0.125-y}Sr_yCuO_4$ ($y = 0.025$ (●), 0.075 (▲)) (left-hand side axis). The diverging character of the associated relaxation rates, σ_1 ($y = 0.025$ (○), 0.075 (△)) marks the magnetic transitions, T_f (right-hand side axis). The lines through the points are guides to the eye.

Figure 6 shows the temperature evolution of the spontaneous precession frequency, ν_μ observed in $La_{1.875}Ba_{0.125-y}Sr_yCuO_4$ ($y = 0.025$ and 0.075). The transition to the magnetically ordered state for $y \leqslant 0.075$ is also depicted by the sudden upturn in the depolarization rates, σ_1 whose absolute value varies with the composition, y and saturates in the mK temperature range $2.5 \leqslant \langle\sigma\rangle \leqslant 3.8\ \mu s^{-1}$.

Above T_f, the muons are depolarized by a distribution of local fields with a zero average internal field strength, $\langle B_\mu\rangle$, but with a non-zero field spread, $\langle\Delta B^2\rangle^{1/2}$. At $T > T_f$, least-squares fits employed the sum of two relaxation functions, one of Gaussian (No 1) and one of Lorentzian (No 2) shape. As shown in figure 5(a) for $La_{1.875}Ba_{0.100}Sr_{0.025}CuO_4$ at $T = 23.6$ K and figure 5(b) for $La_{1.875}Ba_{0.050}Sr_{0.075}CuO_4$ at $T = 14.8$ K, the Gaussian field distribution is necessary to describe the rapid loss of the muon spin polarization, especially at short times, only in a very narrow temperature range of about 5–10 K, just above the freezing temperature. It appears to arise from those domains responsible for the precession signal below T_f and indicates a precursor state for the μ^+ which may involve extremely short-range quasi-static magnetic order. The accompanying Lorentzian field distribution is due to the presence of remnant (super)conducting–paramagnetic regions in the sample where the electronic moments fluctuate slowly ($\langle\lambda\rangle \sim 0.25(1)\ \mu s^{-1}$). This two-component behaviour eventually results into a simple Gaussian field distribution at higher temperatures. The latter is essentially temperature independent, $\langle\sigma_1\rangle \sim 0.23(2)\ \mu s^{-1}$ for all compositions studied. Comparison with other CuO_2-based compounds suggests that σ arises from a field spread (∼2.7 G), characteristic of nuclear dipolar fields of Cu nuclei.

In the present case the temperature evolution of the time-dependent oscillating ZF-μ^+SR signals and the shape of the fairly broad field distribution (FWHM ∼ 75 G) in their Fourier transforms (figure 7) resemble the behaviour observed in the μ^+SR spectra of the incommensurate spin-density wave (SDW) organic system $(TMTSF)_2PF_6$ [36]. The fairly abrupt change near the freezing temperature, T_f is also reminiscent of the SDW transition

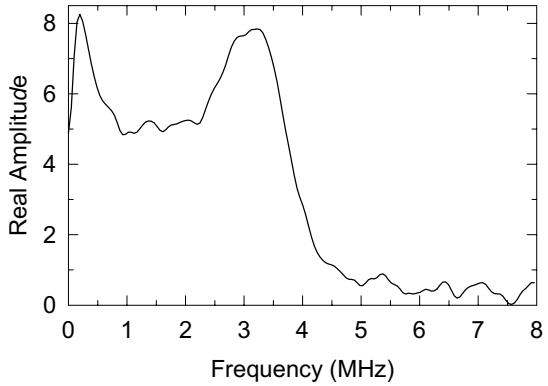

Figure 7. The broad internal field distribution for $La_{1.875}Ba_{0.100}Sr_{0.025}CuO_4$ around 3.3 MHz at $T = 60$ mK, derived by a Fourier transform of the corresponding ZF-μ^+SR spectrum.

in the heavy-fermion $CaAl_3$ system [37] and is also suggestive of an incommensurate magnetic structure, described by one $\boldsymbol{q}$ wave-vector as theoretically expected for a J_0 Bessel depolarization function [38]. Therefore, it appears that the Cu^{2+} unpaired spin density undergoes a transition to an antiferromagnetic sinusoidally modulated state at T_f, whose value decreases smoothly with y. The relatively drastic reduction of the internal field strength, $\langle B_\mu \rangle$ occurs at different T_f for the different samples investigated, namely at $T_f \sim 23$ K for $y = 0.025$ and $T_f \sim 11$ K for $y = 0.075$ (figure 6). The magnitude of its saturated value at $T \sim 60$ mK corresponds to an average muon precession frequency which is similar ($\nu_\mu \sim 3.33(4)$ MHz) for all magnetically ordered samples. This indicates that the average staggered magnetic moment per copper site is essentially independent of y, reaching saturation in the mK temperature range. As the overall hole-doping level is kept constant at $\sim 1/8$, the internal field at the μ^+-stopping sites has a comparable size of $\langle B_\mu \rangle (T \to 0) \approx 245(3)$ G for all compositions. The progressively reduced T_f with increasing y in $La_{1.875}Ba_{0.125-y}Sr_yCuO_4$ (figure 6) suggests that the coherent character of the order of the local magnetic moments is suppressed. On moving from the Ba-rich end of the solid solutions to the Sr-rich one, the relative strength of the superexchange interactions is substantially weakened but not the actual magnitude of the staggered moment per copper site, in agreement with earlier studies of other hole-doped La_2CuO_4 cuprates [39, 40].

3.4. The inhomogeneous microstructure

The stripe model for copper oxide superconductors was developed following neutron [14] and hard-x-ray [41] diffraction studies which showed that in the LTT structure significant incommensurate magnetic and nuclear Bragg peaks are indicative of strong periodic modulations of ordered charge stripes, separated by narrow antiphase antiferromagnetic domains. Related arguments for the present materials can arise from the incomplete nature of their transformation, which is evident in the temperature dependence of the normalized zero-time μ^+SR asymmetries (figure 8). It is worth noting that this mirrors the temperature evolution of the phase fractions in the neutron powder diffraction experiments. The neutron diffraction work suggested that an inhomogeneous microstructure (figure 4) must be present in these materials below the onset of the LTO to LTT transition. ZF-μ^+SR cannot directly sense the charge modulation in $La_{1.875}Ba_{0.125-y}Sr_yCuO_4$. However, it can indirectly probe

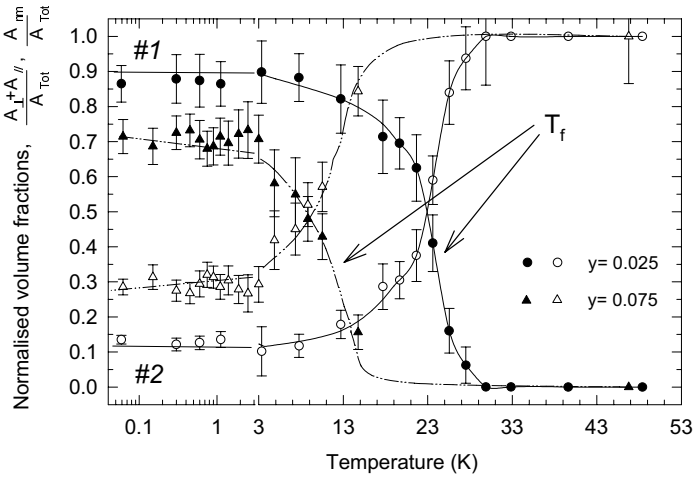

Figure 8. Temperature dependence of the normalized zero-time asymmetry for the ZF-μ^+SR spectra of $La_{1.875}Ba_{0.125-y}Sr_yCuO_4$, showing the different sources of μ^+-spin depolarization: $(A_\perp + A_\parallel)/A_{Tot}$, the spin-density-wave (SDW) volume fraction (component No 1) and A_{nm}/A_{Tot}, the paramagnetic–superconducting volume fraction (component No 2). The lines through the data points are guides to the eye.

the involvement of an additional volume fraction, A_{nm} (No 2) well below the LTO $\rightarrow$ LTT transition, T_{d2}, as the incommensurate magnetically ordered state grows at the expense of the non-magnetic component No 2. Figure 8 demonstrates the correlation among the different sources of μ^+-spin depolarization. Even as $T \rightarrow 0$ K, there is a non-vanishing sample volume (No 2) which shows fairly slow spin fluctuations ($\langle\lambda_3\rangle \sim 1.0(4)$ μs^{-1} at $\sim$3.0 K), as there are remnant LTO microdomains (figure 4) revealed by the Rietveld analysis. The magnetically ordered fraction of muons (No 1) increases fairly quickly and smoothly only well below the structural transition temperature, T_{d2}, determined by our neutron powder diffraction experiments. The μSR results imply that although the total hole doping level is at $\sim 1/8$, the increase in y gradually promotes the stabilization of the LTO microstructure which favours *dynamical* [42] charge and spin correlations instead of the *static* ones [14] encountered for the LTT structure.

The behaviour of the volume fractions should be rationalized by keeping in mind the inhomogeneities resolved by neutron diffraction. Assuming that the magnetically ordered phase is related to the LTT volume fraction, then according to the neutron work only a portion, $(A_\perp + A_\parallel)$ of A_{Tot} goes into the ordered state (figure 8). Electron microscopy studies [30] of $La_{1.8}Ba_{0.12}CuO_4$ found that LTO-2 microdomains (space group $Pccn$) may be present just below the structural transition temperature $T_{d2} \approx 60$ K. The authors proposed that the LTT phase appears to 'nucleate' at and grow out of the LTO twin boundaries, suggesting that an orthorhombic $Pccn$ structure is located at this LTT/LTO interphase region, acting as a buffer structure. This complex microstructure in the present series develops with increasing Sr:Ba ratio. Three-phase Rietveld analysis (table 1) of the neutron diffraction data for $La_{1.875}Ba_{0.025}Sr_{0.100}CuO_4$ confirms the presence of the LTO-2 phase as the majority volume fraction. The ZF-μ^+SR results for this material show no coherent precession of the muon spin, but instead assign LTO-2 as responsible for the existence of a very fast relaxing component (see section 3.5 below), reminiscent of the fast relaxation of component No 1 in compositions with $y \leqslant 0.075$.

The behaviour of the ZF-μ^+SR depolarization rates and especially that related to component No 1 suggests that the $La_{1.875}Ba_{0.125-y}Sr_yCuO_4$ series exhibits a similar complex microstructure. The gradual but rapid increase of the corresponding depolarization rate, σ_1, while approaching T_f from above (figure 6), postulates that a random spin arrangement of *quasi-static* character dominates over the fluctuations of the magnetic moments in the LTO-2 volume fraction. This volume fraction cannot be resolved in component No 1 from that of the purely LTT-static regions, but should develop below T_{d2} as it plays an important role in the kinetics [30] for the formation of the LTT structure. Our observations imply a 'continuous' phase transition of the form LTO $\rightarrow$ (LTO-2) $\rightarrow$ LTT, with the LTO-2 phase characterized by fast relaxation, contributing to the rapid depolarization of component No 1.

3.5. Composition dependent effects—superconductivity

On the assumption that the LTT structure nucleates [30] from the LTO twin boundaries which correspond to the LTO-2 microdomains, we collected ZF-μ^+SR data down to 68 mK for superconducting ($T_c \approx 28$ K) $La_{1.875}Ba_{0.025}Sr_{0.100}CuO_4$. In this case, no evidence of magnetic long-range order was found. Characteristic time-dependent spectra at selected temperatures, $T = 68$ mK and 6 K, together with their two-component fits, of the general form: $P_\mu(t) \sim A_1 \exp(-\frac{1}{2}\sigma_1^2 t^2) + A_2 \exp(-\lambda_2 t)$ are shown in figure 9. What is apparent is the growth of the volume fraction of the Gaussian field distribution (component No 1) on lowering the temperature and its effective fast depolarization ($\sigma_1 \sim 10.3(9)$ μs^{-1} at $T \approx 6.0$ K) of the muon spin. This type of internal field distribution may be expected from a dense spin-glass-like arrangement of magnetic moments [25]. In the present case the corresponding field spread at low temperatures is $\langle \Delta B^2 \rangle^{1/2} \sim 120$ G. The *quasi-static* character of depolarization was confirmed by performing longitudinal-field (LF-) μ^+SR measurements at 5 kG (figure 9). Figure 10 shows that the quasi-static volume fraction (No 1) of the material gradually grows below $T_f \sim 10$ K at the expense of the paramagnetic (but superconducting) slowly relaxing part (No 2) ($\lambda_2 \sim 0.149(5)$ μs^{-1} at $T \approx 6.0$ K). The temperature evolution of the ZF-μ^+SR depolarization rate of the fast component (No 1) diverges while approaching $T \sim 10$ K from below (inset, figure 10). We conclude that the incommensurate SDW state of copper moments disappears at $y \sim 0.100$, in excellent agreement with the substantial diminution of the LTT phase at the same composition, the appearance of the LTO-2 phase and the simultaneous recovery of T_c to $\sim$28 K [19]. In the LTO-2 phase, the tilt pattern of the CuO_6 octahedra is such that static antiferromagnetic spin stripes cannot be pinned down and induce charge segregation, but instead a quasi-static magnetic behaviour is established in a fashion analogous to $La_{1.4}Nd_{0.4}Sr_{0.2}CuO_4$ [43].

The interplay of the physical mechanisms involved in $La_{1.875}Ba_{0.125-y}Sr_yCuO_4$ was also demonstrated by field-cooled ($B_{ext} = 6$ kG) transverse field (TF-) μ^+SR experiments. The measured asymmetries of the TF-μ^+SR time-dependent spectra were fitted, for simplicity, to a Gaussian envelope of the form: $P_\mu(t) \sim \exp(-\frac{1}{2}\sigma_{obs}^2 t^2)\cos(2\pi\nu_\mu t + \phi)$ [44]. The observed relaxation rate, σ_{obs}, includes contributions from both randomly oriented nuclear dipole moments, σ_N ($\approx$0.14 μs^{-1} at 100 K) and flux lattice inhomogeneities, σ. The latter can be estimated from: $\sigma^2 = \sigma_{obs}^2 - \sigma_N^2$ and increases gradually below the superconducting transition temperature, T_c.

In order to account better for the *inhomogeneous* behaviour already confirmed by both neutron diffraction and ZF-μ^+SR, namely the existence of *superconductivity* and *magnetism* in different volume fractions of the materials, the TF-μ^+SR spectra at $T < T_c$ were finally modelled by two-component fits of the above functional form. The temperature dependence

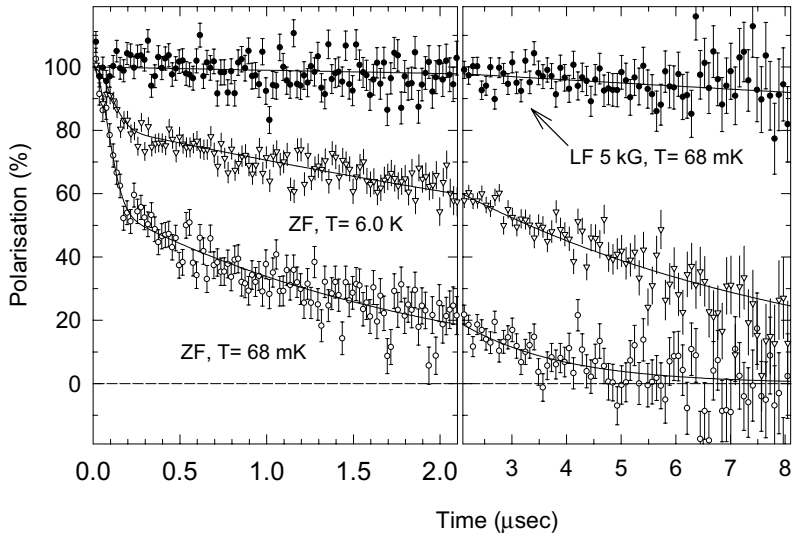

Figure 9. Evolution of the μ^+-spin polarization, $P_\mu(t)$ in $La_{1.875}Ba_{0.100}Sr_{0.025}CuO_4$ at zero field (open symbols) and 5 kG longitudinal field (full symbols), at selected temperatures below the magnetic transition at $T_f \sim 10$ K.

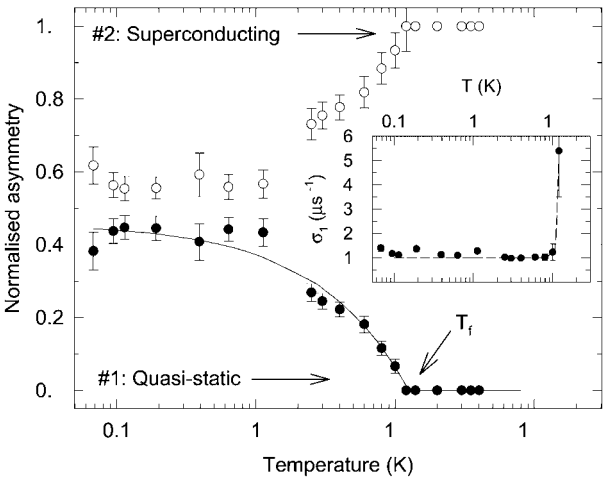

Figure 10. Temperature evolution of the normalized zero-time amplitudes of the two components in the ZF-μ^+SR spectra of $La_{1.875}Ba_{0.025}Sr_{0.100}CuO_4$. The amplitudes are associated with the fractions of the muons due to randomly frozen (No 1: quasi-static) and paramagnetic (No 2: superconducting) spin states. The inset shows the depolarization rate, σ_1 of the quasi-static component No 1.

of $\sigma(T)$ for the *slowly* relaxing component is shown in figure 11(a). The variation of the local field at the muon site due to the Meissner effect below T_c is measured by the frequency shift due to flux expulsion ($\Delta\nu = \nu_\mu - \nu_{ext} = \gamma_\mu \Delta B_\mu$) and is shown for $La_{1.875}Ba_{0.025}Sr_{0.100}CuO_4$ in figure 11(b). The accompanying fast relaxing component, also of Gaussian shape, models the effect of the quasi-static behaviour in a fashion similar to that revealed by our ZF-μ^+SR results, and now presents a rapid depolarization of $\sim$5.1(2) μs^{-1} (at 2.5 K). Depending

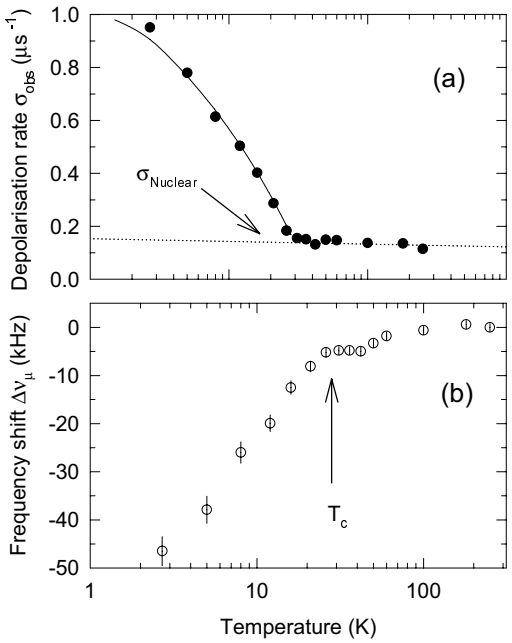

Figure 11. Temperature dependence of (a) the slow relaxation rate, σ_{obs} above and below T_c and (b) the diamagnetic frequency shift, $\Delta\nu_\mu = \nu_\mu - \nu_{ext}$ ($= \gamma_\mu \Delta B_\mu$) at the muon site, as derived for $La_{1.875}Ba_{0.025}Sr_{0.100}CuO_4$ by transverse-field (TF-) μ^+SR scans at $B_{ext} = 6$ kG.

on the theoretical model [21, 22] used to describe the field distribution in the vortex state, the proportionality constant between the London penetration depth, λ and σ takes different values. We used the convention $\lambda = a\sigma^{-1/2}$ [24] and the Brandt model ($\alpha = 3270$) to extract values of the penetration depth from the TF slow relaxation rates, for the Ba-rich ($y = 0.0$) $\lambda_{T\sim 5\ K} = 5390(325)$ Å and Ba-poor ($y = 0.1$) $\lambda_{T\sim 5\ K} = 3760(50)$ Å materials. It appears that λ increases with decreasing y, reflecting the growth of static magnetic correlations below T_{d2}, and the magnetic pair-breaking effect of the LTT phase.

Figure 8 displays the temperature and composition evolution of the microscopic sources of the ZF μ^+-spin depolarization. It shows the behaviour of the superconducting (No 2) and the quasi-static conducting, interphase regions due to LTO-2 phase (hidden in No 1) of the samples. The overall picture is that both the fluctuating (No 2) and slowed down (hidden in No 1, while approaching T_f) local fields progressively extend to an increased proportion of the sample volume with increasing y and become the dominant contributions for the muon depolarization at $y > 0.075$. Thus the overall dynamic-like modulations of the spin and charge density in the LTO and LTO-2 (super)conducting microdomains are frozen and become static as the penetration depth, λ becomes longer in the Ba-rich samples. The ratio of the superconducting carrier density over the effective mass, $\sigma \propto \lambda^{-2} \propto n_s/m^*$ [23, 24] is then effectively reduced due to the gradual appearance of the long-range magnetic order. The spatial modulation of the spin and charge densities mimics the stripe-phase correlations revealed by muon spin relaxation data [10, 43] in the magnetically ordered phase of the LTT structure in $La_{1.6-y}Nd_{0.4}Sr_yCuO_4$. Analogous arguments were employed in a combined NQR and μ^+SR study [41] in order to rationalize the suppression of the Néel state with increasing hole-content in lightly doped $La_{2-x}Sr_xCuO_4$ ($x < 0.02$) phases.

4. Conclusions

We have presented ZF-μSR measurements at low temperatures on the compositions $La_{1.875}Ba_{0.125-y}Sr_yCuO_4$ ($0 \leqslant y \leqslant 0.1$). The results were discussed by taking into account the findings of complementary neutron powder diffraction measurements on the same samples. The materials, with an average hole-doping level of 1/8, show inhomogeneous microstructures. For compositions with $y \leqslant 0.075$, residual micro-strain effects accompany the LTO $\rightarrow$ LTT structural transformation at T_{d2}, as evidenced by the presence of strong broadening of the Bragg peaks. Temperature dependent neutron diffractometry down to 4.5 K and use of Rietveld analysis show that the inhomogeneous structure found on approaching T_{d2} is accompanied by a fairly rapid increase of the LTT volume fraction and simultaneous reduction, but not disappearance, of the orthorhombicity in the LTO phase. Full profile analysis of the neutron diffraction pattern for $y = 0.100$ at 4.5 K revealed a less orthorhombically distorted LTO-2 structure (space group $Pccn$), which appears to play an important role in controlling the appearance of the LTT phase. It behaves like a buffer structure such that the LTO $\rightarrow$ LTT transition occurs via LTO-2 in a fashion similar to $La_{1.8}Ba_{0.12}CuO_4$ [30]. Our earlier TF-μ^+SR results on $La_{1.875}Ba_{0.075}Sr_{0.050}CuO_4$ [16] had given evidence for the presence of a component of magnetic origin. The present multicomponent behaviour in $La_{1.875}Ba_{0.125-y}Sr_yCuO_4$ implies that the same spatially inhomogeneous features are present in all samples.

The results down to the mK temperature range have shown that diminution of superconductivity with increasing Ba content in this system is associated with the pinning of antiferromagnetic spin domains in the LTT structure. Such a description is reminiscent of the phase separation phenomenology [13] in cuprate superconductors. Static magnetic interactions for the Ba-rich materials dominate the majority of the sample volume at low temperatures and build up in strength below the structural transition at T_{d2}. As $T \rightarrow 0$ K, there is always a non-vanishing sample volume, which shows slow spin fluctuations, in agreement with the presence of remnant LTO superconducting microdomains. Finally, the presence of an additional component, which exhibits relatively fast fluctuations of the moments is identified with the LTO-2 microdomains. This shows an enhanced depolarization rate close to the freezing temperature, T_f, supporting a quasi-static character for the moments. The LTO-2 magnetic interactions 'prepare' the materials in order to pass to the long-range magnetically ordered state. The static spin correlations are, in turn, sensitively affected by the increase in the Sr content, y, and disappear at $y = 0.100$ when the LTT phase becomes suppressed. Instead a quasi-static component, associated with the LTO-2 regions grows at the expense of the superconducting part (LTO) of the material.

Thus the overall dynamic-like modulations of the spin and charge density in the LTO-2 and LTO domains acquire mainly static character with increasing Ba content. The resulting long-range magnetic order appears to have a pair-breaking effect inferred from the lengthening of the London penetration depth associated with the reduction in the superconducting carrier density in the LTT materials. The spatial modulation of the spin and charge densities mimics the stripe-phase correlations revealed by muon spin relaxation data in the magnetically ordered phase of the LTT structure, as in other related materials [10, 43].

Acknowledgments

We thank EPSRC for financial support and access to the neutron facilities at ISIS and R M Ibberson for invaluable help with the HRPD experiments. Financial support from the British Council, the Swiss NSF and the TMR Programme of the European Commission (Research Network 'FULPROP' ERBFMRXCT970155) is acknowledged. We also thank

the Paul Scherrer Institute for the provision of muon beam time, A Amato, C Baines and R Feyerherm for help with the μ^+SR experiments and D Herlach for technical support.

References

[1] Birgeneau R J *et al* 1987 *Phys. Rev. Lett.* **59** 1329
[2] Axe J D, Moudden A H, Hohlwein D, Cox D E, Mohanty K M, Moodenbaugh A R and Xu Y 1989 *Phys. Rev. Lett.* **62** 2751
[3] Cox D E, Zolliker P, Axe J D, Moudden A H, Moudenbaugh A R and Xu Y 1989 *Mater. Res. Soc. Symp. Proc.* vol 156 (Pittsburgh, PA: Materials Research Society) p 141
[4] Moodenbaugh A R, Xu Y, Suenaga M, Folkerts T J and Shelton R N 1988 *Phys. Rev.* B **38** 4596
Sera M, Ando Y, Kondoh S, Fukuda K, Sato M, Watanabe I, Nakashima S and Kumagai K 1989 *Solid State Commun.* **69** 851
[5] Kumagai K, Kawano K, Watanabe I, Nishiyama N and Nagamine K 1994 *Hyperfine Interact.* **86** 473
[6] Luke G M, Le L P, Sternlieb B J, Wu W D, Uemura Y J, Brewer J H, Riseman T M, Ishibashi S and Uchida S 1991 *Physica* C **185–189** 1175
[7] Rosseinsky M J, Prassides K and Day P 1991 *J. Mater. Chem* **1** 597
[8] Crawford M K, Harlow R L, McCarron E M, Farneth W E, Axe J D, Chou H and Huang Q 1991 *Phys. Rev.* B **44** 7749
[9] Buchner B *et al* 1991 *Physica* C **185–189** 903
Buchner B *et al* 1993 *Europhys. Lett.* **21** 953
[10] Wagener W, Klaus H H, Hillberg M, de Melo M A C, Birke M, Litterst F J, Buchner B and Micklitz H 1997 *Phys. Rev.* B **55** 14 761
[11] Pickett W E, Cohen R E and Krakauer H 1991 *Phys. Rev. Lett.* **67** 228
[12] Bonesteel N E, Rice T M and Zhang F C 1992 *Phys. Rev. Lett.* **68** 2684
[13] Phillips J C 1993 *Phys. Rev.* B **47** 2944
[14] Tranquada J M, Sternlieb B J, Axe J D, Nakamura Y and Uchida S 1995 *Nature* **375** 561
Tranquada J M, Axe J D, Ichikawa N, Nakamura Y, Uchida S and Nachumi B 1996 *Phys. Rev.* B **54** 7489
[15] Emery V J and Kivelson S A 1993 *Physica* C **209** 597
[16] Maeno Y, Odagawa A, Kakehi N, Suzuki T and Fujita T 1991 *Physica* C **173** 322
[17] Lappas A, Cristofolini L, Prassides K, Vavekis K, Amato A, Gygax F N, Pinkpank M and Schenck A 1997 *Hyperfine Interact.* **105** 101
[18] Larson A C and von Dreele R B 1994 General Structure Analysis System *Los Alamos National Laboratory Report* LAUR 86-748
[19] Lappas A 1993 *DPhil Thesis* University of Sussex p 323
[20] Lappas A, Osborne J, Prassides K, Amato A, Feyerherm R, Gygax F N and Schenck A 1994 *Physica* B **194–196** 353
[21] Pincus P, Gossard A C, Jaccarino V and Wernick J H 1964 *Phys. Lett.* **13** 31
[22] Brandt E H 1988 *Phys. Rev.* B **37** 2349
[23] Keller H 1989 *IBM J. Res. Dev.* **33** 314
[24] Uemura Y J *et al* 1991 *Nature* **352** 605
Nachumi B, Keren A, Kojima K, Larkin M, Luke G M, Merrin J, Tchernyshov O and Uemura Y J 1996 *Phys. Rev. Lett.* **77** 5421
[25] Schenck A 1993 *Frontiers in Solid State Sciences* vol 2, ed L C Gupta and M S Multani (Singapore: World Scientific) p 269
[26] Ganguly P and Rao C N R 1984 *J. Solid State Chem.* **53** 193
[27] Hatch D M, Stokes H T, Alexandrov K S and Misyul S V 1989 *Phys. Rev.* B **39** 9282
[28] Axe J D 1992 *Proc. Conf. on Lattice Effects in High-T_c Superconductors* ed Y Bar-Yam, T Egami, J Mustre-de Leon and A R Bishop (Singapore: World Scientific) pp 517–30
[29] Buchner B, Breuer M, Freimuth A and Kampf A P 1994 *Phys. Rev. Lett.* **73** 1841
[30] Zhu Y, Modenbaugh A R, Cai Z X, Tafto J, Suenaga M and Welch D O 1994 *Phys. Rev. Lett.* **22** 3026
[31] Billinge S J L, Kwei G H, Lawson A C, Thompson J D and Takagi H 1993 *Phys. Rev. Lett.* **71** 1903
[32] Rodríguez-Carvajal J, Fernández-Diaz M T and Martínez J L 1991 *J. Phys.: Condens. Matter* **3** 3215
[33] Hara N, Kamiyama T, Kamata I, Nakahara I, Hayakawa H, Akiba E and Asano H 1992 *Solid State Commun.* **82** 975
[34] Lappas A, Osborne J, Prassides K, Amato A, Feyerherm R, Gygax F N and Schenck A 1994 *Physica* C **235–240** 1725

[35] Barth S, Ott H R, Gygax F N, Hitti B, Lippelt E, Schenck A and Baines C 1987 *Phys. Rev. Lett.* **59** 2991
[36] Le L P *et al* 1993 *Phys. Rev.* B **48** 7284
[37] Amato A 1997 *Rev. Mod. Phys.* **69** 1119
[38] Major J, Mundy J, Schmolz M, Seeger A, Doring K P, Furderer K, Gladisch M, Herlach D and Majer G 1986 *Hyperfine Interact.* **31** 259
[39] Uemura Y J *et al* 1988 *Physica* C **153–155** 769
[40] Borsa F *et al* 1995 *Phys. Rev.* B **52** 7334
[41] Zimmermann M V *et al* 1998 *Europhys. Lett.* **41** 629
[42] Cheong S-W, Aeppli G, Mason T E, Mook H, Hayden S M, Canfield P C, Fisk Z, Clausen K N and Martinez J L 1991 *Phys. Rev. Lett.* **67** 1791
Mason T E, Aeppli G and Mook H A 1992 *Phys. Rev. Lett.* **68** 1414
[43] Nachumi B *et al* 1998 *Phys. Rev.* B **58** 8760
[44] Riseman T M *et al* 1995 *Phys. Rev.* B **52** 10 569